Ocular aberrations with ray tracing and Shack–Hartmann wave-front sensors: Does polarization play a role?

Susana Marcos

Instituto de Optica "Daza de Valdés," Consejo Superior de Investigaciones Científicas, Serrano 121, Madrid, 28006 Spain

Luis Diaz-Santana

Applied Vision Research Centre, Department of Optometry and Visual Science, City University, Northampton Square, London EC1V 0HB, UK

Lourdes Llorente

Instituto de Optica "Daza de Valdés," Consejo Superior de Investigaciones Científicas, Serrano 121, Madrid, 28006 Spain

Chris Dainty

Blackett Laboratory, Imperial College, London SW7 2BW, UK

Received July 6, 2001; revised manuscript received January 3, 2002; accepted January 7, 2002

Ocular aberrations were measured in 71 eyes by using two reflectometric aberrometers, employing laser ray tracing (LRT) (60 eyes) and a Shack–Hartmann wave-front sensor (S–H) (11 eyes). In both techniques a point source is imaged on the retina (through different pupil positions in the LRT or a single position in the S–H). The aberrations are estimated by measuring the deviations of the retinal spot from the reference as the pupil is sampled (in LRT) or the deviations of a wave front as it emerges from the eye by means of a lenslet array (in the S–H). In this paper we studied the effect of different polarization configurations in the aberration measurements, including linearly polarized light and circularly polarized light in the illuminating channel and sampling light in the crossed or parallel orientations. In addition, completely depolarized light in the imaging channel was obtained from retinal lipofuscin autofluorescence. The intensity distribution of the retinal spots as a function of entry (for LRT) or exit pupil (for S–H) depends on the polarization configuration. These intensity patterns show bright corners and a dark area at the pupil center for crossed polarization, an approximately Gaussian distribution for parallel polarization and a homogeneous distribution for the autofluorescence case. However, the measured aberrations are independent of the polarization states. These results indicate that the differences in retardation across the pupil imposed by corneal birefringence do not produce significant phase delays compared with those produced by aberrations, at least within the accuracy of these techniques. In addition, differences in the recorded aerial images due to changes in polarization do not affect the aberration measurements in these reflectometric aberrometers.

OCIS codes: 330.5370, 260.5430.

1. INTRODUCTION

The fact that the eye suffers from optical aberrations has been known for more than a century. However, in recent years, the measurement of ocular aberrations has experienced an unprecedented interest, drawn by the development of new instrumentation and by the increasing possibilities for compensation of terms beyond conventional refractive errors.[1–6]

Both psychophysical[7] and reflectometric techniques[8–12] are being used currently to measure ocular wave aberrations. It has been demonstrated that within the accuracy of each method the two types of measurements provide similar wave aberration estimates in normal eyes.[13,14] However, the increased speed of the latter make them more attractive in a clinical environment or in applications in which data collection speed is required. In reflectometric techniques the light reflected back from the retina is collected on a CCD camera, generally in a plane conjugate to the retina. A possible concern in these techniques is whether the interaction of the light with the different retinal layers can play a role in determining the aberration pattern. Factors that can affect the amount of light sampled include wavelength and polarization state (of the illumination and detection channels).

From studies of the spectral reflectance of the fundus,[15] it has been found visible light is more likely to be reflected by the photoreceptor outer segments, whereas near-infrared (IR) light is reflected more by deeper layers (retinal pigment epithelium and choroid). Wavelength differ-

ences in reflectivity of different retinal layers do not seem to affect the aberration pattern measured.[16,17] Except for the defocus term, whose difference is consistent with the chromatic difference in focus,[18–20] no significant differences are found with use of IR or green light.[16,17]

Polarized light also interacts with the ocular optical components and the retina. There are several reasons to study whether the polarization of the incident (and the returning light in the imaging systems) may affect aberration measurements:

1. Corneal birefringence,[21] and to a lesser extent the crystalline lens[22] and the retina (effect probably negligible at the central fovea), produces a retardation of linearly polarized light.[23] A mean retardation of 70 deg, which varied across the pupil, was found experimentally with double-pass ellipsometric measurements of the polarization properties of ocular structures.[24] This shift will produce an average phase difference of $\lambda/5$ when changing the polarization of the incident light and/or analyzer in the imaging channel in imaging aberrometers. A recent study[25] using a spatially resolved refractometer (a psychophysical technique) showed no difference in the wave aberration measured with different states of polarization of the illuminating channel. This suggests that the phase shift produced by corneal birrefringence is negligible in terms of wave-front error compared to phase distortions produced by other structural properties of the ocular components.

2. The use of polarizers in the illumination and detection channels affects the intensity of the raw data (aerial retinal images captured on a CCD camera). Changes in the polarization state of light passing through the eye produce different intensity patterns after the light passes through an analyzer. These changes of intensity have a large impact on the point-spread-function estimates obtained by using a double-pass arrangement that incorporates a polarizing channel and an analyzer channel. Bueno and Artal[26] used an ellipsometry approach to study the influence of polarization in double-pass estimates of the image quality of the eye. They found that the double-pass aerial image (autocorrelation of the ocular point-spread function[27]) was influenced by the relative orientation of the polarizer and the analyzer (placed in the illumination channel and the imaging channel, respectively). These differences caused significant variations in the resulting modulation transfer function and therefore in the estimated image quality. As opposed to the conventional double-pass technique, the aerial images recorded in laser ray tracing (LRT) or Shack–Hartmann wave-front sensor (S–H) systems are used only to compute the centroid of several intensity patterns. However, relative differences in intensity in the core and tails of the retinal image or differences in shape could result in changes in the estimation of the centroid and have an impact on the wave aberration estimate.

3. Some S–H setups described in the literature use polarized light[8] and in particular, analyze cross-polarized light in the detection channel to attenuate artifacts introduced by the corneal reflex. This study will show whether experimental results from such systems could be affected by the specific configuration.

In the current paper we investigate whether polarization may have an effect in reflectometric measurements of wave aberrations. In particular, we used a LRT[11] and a S–H system,[9] implemented at the Instituto de Optica, Consejo Superior de Investigaciones Científicas, Madrid, Spain, and the Imperial College, London, UK, respectively. The principles of the two techniques are similar, the main differences being that the former is sequential and the measurement is done in the ingoing pass, whereas the second works in parallel and the measurement is done in the outgoing pass.[13] We did not attempt to fully characterize the wave aberration with state of polarization, but rather attempted to test whether some typical combinations of polarization in the incident and detection channels may influence wave aberration measurements. We used linearly and circularly polarized light. These two states of polarization combine differently with retardation across the pupil, producing different phase shifts at different pupil locations. We used parallel and crossed orientations of the polarization state in the imaging and detection channels, which must produce large differences in the relative intensity of the aerial images captured across the pupil. In addition, we generated a completely depolarized source on the retina to test a nonpolarized condition. Our experiments show that these polarization states do not influence reflectometric aberration measurements in the eye, at least within the error of the measurements.

2. METHODS

A. Laser Ray Tracing

1. Setup and Procedures

The LRT technique has been described in detail elsewhere.[13,28–30] In brief, a narrow laser (543-nm) beam scans the eye pupil (6.5-mm diameter, 1-mm step size, 37 samples in a hexagonal arrangement), and the corresponding images of the spot projected on the retina, for each entry pupil, are collected sequentially on a high-resolution imaging CCD with a 3-mm exit pupil. Deviations from the principal ray (estimated by computing the relative position of the image centroids) are proportional to the local slopes of the wave aberration. The slopes are fitted to a 7th-order Zernike polynomial (35 terms), and the wave aberration is computed using a least-mean-square procedure.

2. Experiments

We performed two different experiments: In the first one, we illuminated the eye with linearly polarized light and collected the light linearly polarized in the crossed direction. This was achieved by using a polarizing beam splitter, which reflects linearly polarized light and transmits linearly polarized light rotated 90°. In the second one, a quarter-wave plate was introduced between the beam splitter and the eye. Light in the illumination channel was then circularly polarized. Light emerging from the eye, which preserves its polarization state, was then fully transmitted into the imaging channel. All measurements were done foveally, and with the center of the pupil as the reference axis. For proper alignment

and continuous monitoring, the pupil was illuminated with IR light and viewed on a CCD centered on the optical axis of the instrument.

3. Subjects

Twenty-eight subjects participated in the experiment. Ages ranged from 18 to 46 and refractive errors ranged from −10.47 to 0.68 diopters (D). We report a total of 60 measurements (E#1–E#60). We include both normal and atypically highly aberrated eyes, since the group under test includes 22 eyes at least one month after LASIK surgery, which typically increases the amount of higher-order aberrations.[29] Eleven eyes were tested both before and after LASIK and were considered as independent measurements. All eyes were dilated with one drop of tropicamide 1%, and refractive errors were compensated with trial lenses when necessary. Subjects were stabilized with a dental impression and head rest, and the pupil was continuously monitored to ensure proper alignment. Each measurement consisted of ten runs (37 entry pupils), five runs with crossed linear polarization in the illuminating and imaging channels (experiment 1) and five runs with parallel circular polarization in the illuminating and imaging channel (experiment 2).

B. Shack–Hartmann

1. Setup and Procedures

The implementation of the S–H at Imperial College, London, has been described in detail elsewhere.[31,32] In brief, a collimated laser beam forms a spot on the retina. The emerging beam is sampled by a rectangular lenslet array placed in a plane conjugate to the pupil. Each lenslet is 0.8 mm × 0.8 mm over the eye pupil with 35-mm focal length. The number of sampling lenslets (32–48 lenslets) is defined by the subject's pupil size (ranging from 5 to 6.5 mm). A CCD camera, placed on the focal plane of the lenslet array and conjugated with the retina records the Shack–Hartmann spot pattern. Deviations from the ideal spot pattern are proportional to the local slopes of the wave aberration. The slopes are fitted to a 6th-order Zernike polynomial (27 terms), and the wave aberration is computed using a least-mean-square procedure.

2. Experiments

We performed three different experiments, using different configurations for the state of polarization in the illuminating channel and the state of polarization of the light sampled in the imaging channel. In the first experiment, we illuminated the eye with linearly polarized light (635 nm) and collected the light linearly polarized in the crossed direction by using a polarizing beam splitter, which reflects linearly polarized light and transmits linearly polarized light rotated 90°. In the second experiment, the illumination channel was circularly polarized, and light with the same state of polarization was maximally sampled in the imaging channel. This was achieved by placing a quarter-wave plate between the polarizing beam splitter and the eye. In the third experiment, the eye was illuminated with partially polarized light (from a He–Ne laser at 543 nm), and completely depolarized light was sampled by the imaging channel. To achieve a depolarized state, a fluorescence technique was used.[31,33] Fluorescent light was collected by replacing the beam splitter with a dichroic filter, reflecting the sampling light (543 nm) and transmitting wavelengths other than the excitation wavelength. Fluorescence is known to originate in the lipofuscin molecules at the retinal pigment epithelium.[33] A fluorescent source is equivalent to a perfectly incoherent source. Light is completely unpolarized, and speckle is not present. The peak of the fluorescent spectrum is close to 635 nm. All experiments were done foveally and with pupil centration. Subjects were stabilized with the help of a dental impression. Alignment was achieved by measuring the displacement required for the subject to stop seeing the beam coming into his or her eye on the left, right, top, and bottom and finally computing the pupillary center. For each condition, we obtained at least ten measurements consecutively. The alignment procedure was repeated every ten measurements.

3. Subjects

Eleven normal subjects participated in these experiments. Only left eyes were used (E#61–E#71). Ages ranged between 26 and 52 years. Spherical refractive errors ranged between −3.25 D and 2.25 D. Seven subjects participated in comparative measurements of experiments 1 and 3, two subjects in those of experiments 2 and 3, and two subjects in those of experiments 1 and 2. All eyes were dilated and cyclopleged with one drop of tropicamide 1% and one drop of phenylephrin 2.5%.

C. Comparison of Shack–Hartmann and Laser Ray Tracing Setups

Previous studies have shown that measurements on the same normal subjects using the S–H and LRT provide identical results, within the accuracy of the methods. To test the equivalence of the two systems used in this study, we conducted measurements on two control subjects who traveled between London and Madrid. These subjects did not participate in the full measurements reported in this study and were tested with the standard conditions in each lab. Standard conditions for LRT included 543-nm illumination and random polarization. Standard conditions for the S–H included 543-nm illumination and crossed polarization. Figure 1 shows wave aberration contour plots for the right eyes of both control subjects, for 3rd-order and higher aberrations, for LRT (left panels) and the S–H (right panels). Pupil size was 6.5 mm in the LRT experiment and 6 mm in the S–H experiment. The two systems capture similar wave aberration maps. The larger differences found for control eye #2 are likely due to slight differences in the alignment. Root-mean-square wave-front error for 3rd-order aberrations and higher (computed for 6-mm pupils in both systems) was 0.46 μm and 0.43 μm for LRT and the S–H, respectively for control eye #1, and 0.48 μm and 0.57 μm, respectively, for control eye #2. For both eyes, the spherical aberration 4th-order term was the major contributor to wave-front error: 0.30 μm and 0.33 μm for LRT and the S–H, respectively, for control eye #1, and 0.28 μm and 0.35 μm for LRT and the SH, respectively, for control eye #2.

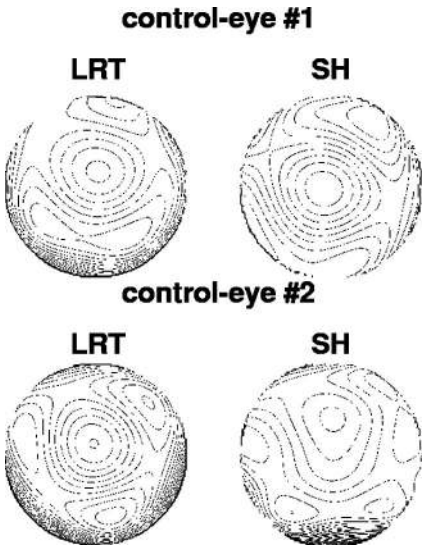

Fig. 1. Wave aberration contour for control eyes measured in both the LRT setup in Madrid (left) and the S–H system in London (right). First- and second-order aberrations have been canceled. Pupil diameter was 6.5 mm for LRT and 6 mm for the S–H. Contour spacing was 0.3 μm.

3. RESULTS

A. Raw Data

LRT captures a set of retinal aerial images of a distant point source as a function of entry pupil position. Figures 2a and 2b show an example of such a series of retinal images for a single run on eye #23 for circularly parallel (a) and linearly crossed (b) polarization conditions. The images have been placed at their corresponding entry pupil position. The shape of aerial images (slightly defocused for this subject) remains approximately constant across the pupil for each condition. The relative intensity of the aerial images across the pupil is different in each condition (brighter in the center in a, and brighter in the corners in b). Polarization conditions may also affect the shape of the aerial images.[34] Figure 2c shows the corresponding retinal spot diagram, i.e., the joint plot of the centroids of the sets of images in a (circles) and b (crosses), for this subject. Data across five consecutive runs have been averaged. The error bars indicate the standard deviation of the angular locations. For most positions, the difference between the two polarization conditions is within the error. Figures 2d and 2e show S–H

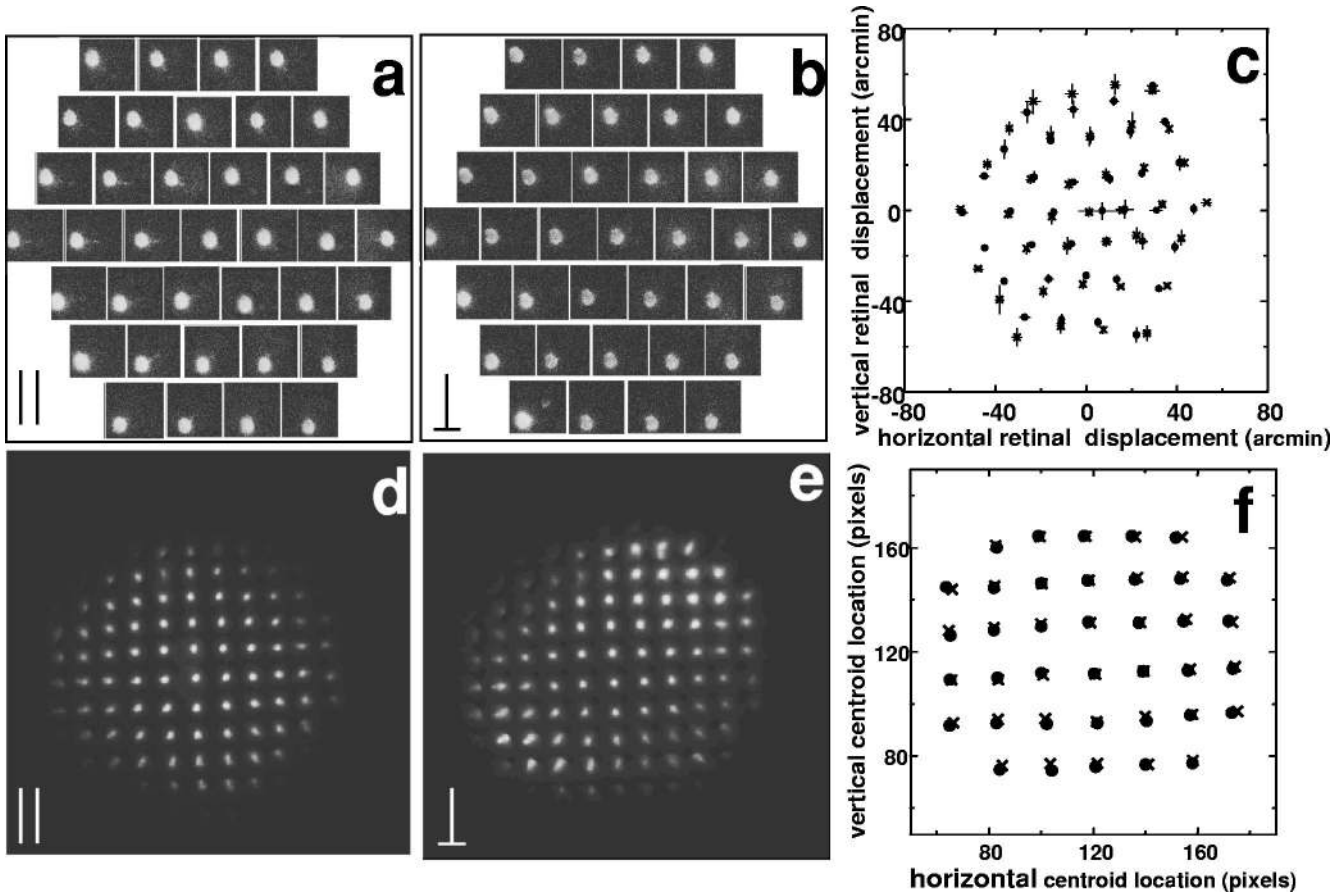

Fig. 2. Raw data as captured by LRT (panels a–c) and the S–H (panels d–f). In LRT a series of retinal images is captured sequentially as a function of entry pupil position. Examples are shown for eye #23 for circular parallel polarization (a) and linear crossed polarization (b). Each image is placed at the corresponding entry location (as looking at the subject's pupil). Panel c shows the corresponding spot diagram (i.e., the joint plot of the centroids of the images shown in a and b). Circles stand for circular parallel polarization and crosses for linear crossed polarization. Panels d and e show S–H images for eye #63 for circular parallel polarization (d) and linear crossed polarization (e). Panel f plots the corresponding centroids of the S–H images; symbol notation is the same as for the spot diagrams in c.

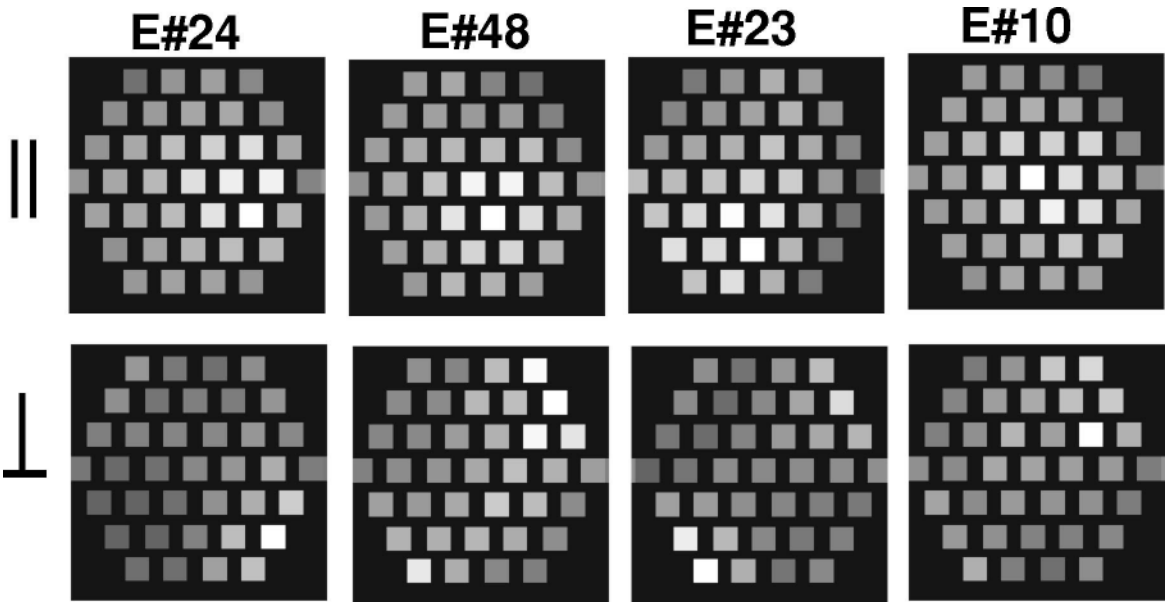

Fig. 3. Pupillary intensity maps computed from the intensity of the LRT aerial images for four eyes (#24, OS; #48, OD; #23, OS; #10, OD). Each square represents the total intensity (average of five runs) of the aerial image of the corresponding pupil position. Upper row, circular polarization in the illumination channel, analyzer in the same orientation. Lower row, linear polarization in the illumination channel, analyzer in the crossed orientation. Pupil position range from −3 to +3 mm. Positive horizontal positions indicate nasal positions in right eyes and temporal positions in left eyes, and positive vertical positions indicate superior pupil.

images for circularly parallel (d) and linearly crossed (e) polarization conditions, for eye #63. Figure 2f shows the S–H centroids corresponding to d (circles) and e (crosses). Despite the difference in brightness between the two S–H images, the centroid locations are similar.

B. Intensity Patterns

Both LRT and the S–H capture a set of retinal images as a function of pupil position (entry pupil position for LRT and exit pupil position for the S–H). The modulation of the intensity of these retinal images as a function of pupil position can be regarded as a pupillary intensity pattern. This modulation depends on both the pupil relative luminous efficiency, in the case of light interacting with cone photoreceptors,[35] and the interaction of the state of polarization with birefringence properties (particularly those of the cornea[21,36,37]). Relative differences of the state of polarization of the illumination and imaging channels produce differences in the intensity captured on the CCD as well as on the intensity pattern across the pupil.

Figure 3 shows pupillary intensity patterns corresponding to experiments 1 and 2 produced by LRT for four individual eyes (#24, #48, #23, #10). Each square represents the total intensity (average of five runs) of the aerial image of the corresponding pupil position. Pupil position range from −3 to +3 mm both horizontally and vertically. Positive horizontal positions indicate nasal positions in right eyes and temporal positions in left eyes, and positive vertical positions indicate superior pupil. For each subject, we show data corresponding to the two polarization combinations (crossed linearly polarized—experiment 1—and parallel circularly polarized—experiment 2), collected consecutively while the rest of experimental conditions were kept identical. Each image is normalized to the maximum intensity value of the series. The intensity distribution changes completely depending on the polarization combination. The crossed polarization patterns (Fig. 3, lower row) show a dark area in the central pupil and bright areas at the corners of the pupil. It resembles the corneal cross, vigneted by the edges of the pupil, or the hyperbolic shape associated with corneal birrefringence and observed when the cornea is imaged through two crossed polarizers.[21,36,37] Retinal polarization effects are probably irrelevant, since the foveal area sampled (a few arc min) is much smaller than the retina brushlike patterns (4–5°) observed in retinal photographs between polarizers, which are attributed mainly to the retinal fiber layer. In addition, retardation by photoreceptors as suggested by Hocheimer and Kues[38] has been proved small.[24] As found in previous studies,[21] these intensity patterns show bilateral mirror symmetry (Fig. 4, for right and left eye of the same subject). The parallel

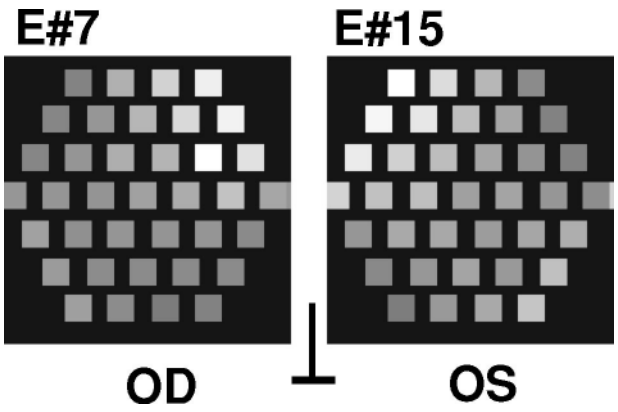

Fig. 4. Pupillary intensity maps (computed from LRT aerial images, as in Fig. 3) for right (E#7) and left (E#15) eyes of the same subject, using linear polarization in the illumination channel and analyzer in the crossed orientation. The maps show a dark central area and bright nasal-superior corners, and they are bilaterally symmetric.

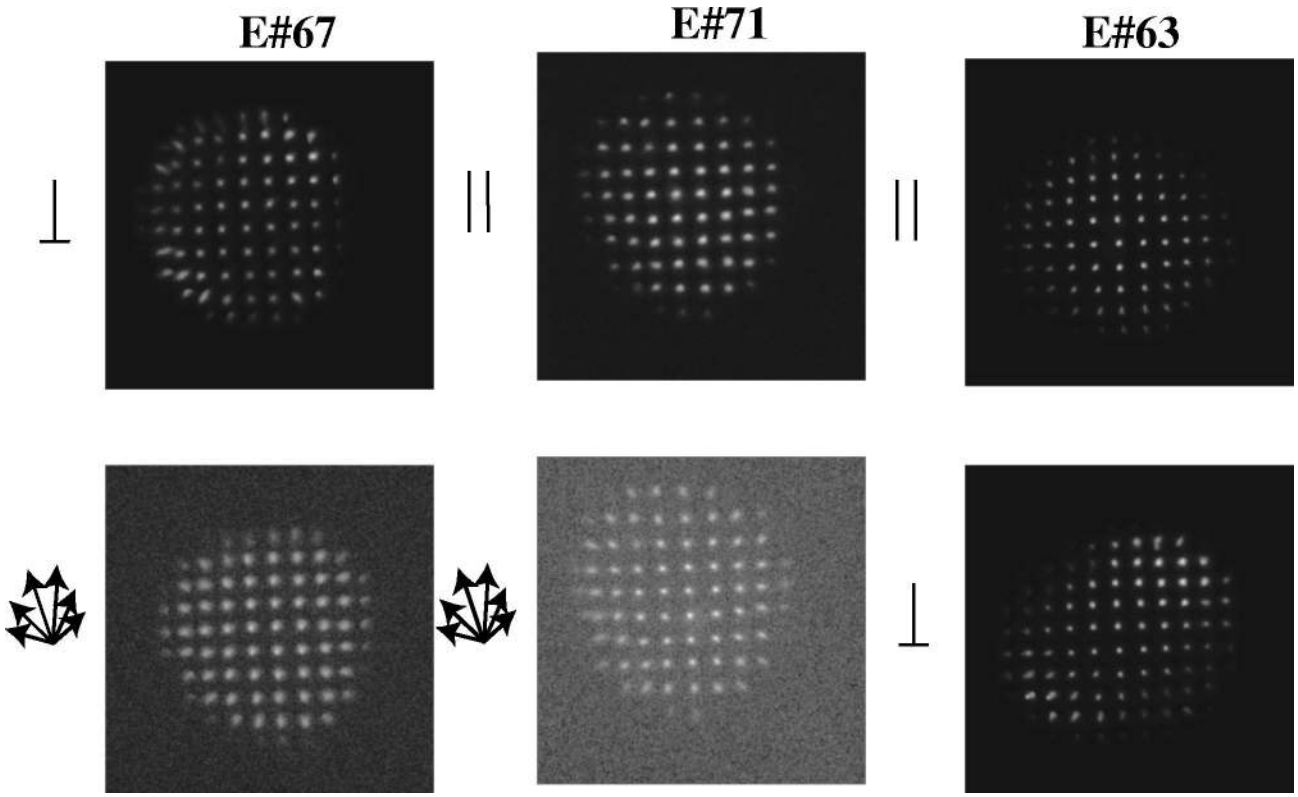

Fig. 5. Shack–Hartmann spot image for eyes #67 (OS), #71 (OS), #63 (OS). The left panels compare linear polarization in the illumination channel and analyzer in the crossed orientation (top) with autofluorescence (totally depolarized) sampled light (bottom). The middle panels compare circular polarization in the illumination channel and analyzer in the parallel orientation (top) with autofluorescence (bottom). The right panels compare circular parallel (top) with linear crossed polarizations (bottom). Positive horizontal positions indicate temporal pupil positions, and positive vertical positions indicate superior pupil.

circularly polarized patterns (Fig. 3, upper row) show a bright area in the central part of the pupil, with the location of the maximum depending on the subject and the relative intensity decreasing toward the margins of the pupil. This Gaussian distribution is very likely associated with directionality properties of the cone photoreceptors.[35,39,40] Figure 5 shows the S–H spot patterns, for three eyes (all left eyes). Upper and lower rows represent data corresponding to different conditions of polarization state. Left panels show cross-polarized and autofluorescence patterns for eye #67, middle panels show parallel circular polarization and autofluorescence for eye #71, and right panels show parallel circular and crossed polarizations for eye #63. Intensity patterns in the cross-polarized and parallel circular conditions are similar to those described for Fig. 3. The autofluorescence spot patterns show the most homogeneous intensity distribution, consistent with the fact that cones do not recapture light scattered by lipofuscin.[41]

C. Wave Aberration Patterns

Figure 6 shows contour plots of the wave aberration corresponding to the four typical eyes and the two experimental conditions shown in Fig. 3, measured by LRT. Each map is the average of at least three experimental runs. Tilt and defocus were set to zero. Eyes #24 (OS) and #48 (OD) are eyes following LASIK refractive surgery; Eyes #23 (OS) and #10 (OD) are normal eyes. Figure 7 shows contour plots of the wave aberration corresponding to three eyes measured with the S–H (#67, #71, and #70). Wave aberration patterns do not show significant changes when the state of polarization of the incident and/or the sampled light is varied.

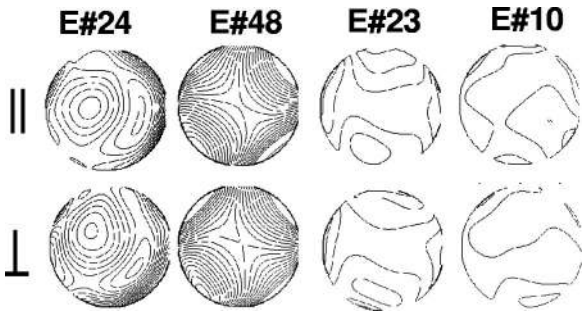

Fig. 6. Wave aberration contour maps for eyes #24, #48, #23, and #10, measured with LRT. Lines are plotted every 1 μm. Upper and lower panels as in Fig. 3. Defocus has been canceled. Pupil diameter was 6.5 mm for all eyes.

D. Zernike Coefficients

Figure 8 shows examples of comparisons of Zernike coefficients measured with different pairs of polarization states for one of the eyes shown in Fig. 6 and the three eyes of Fig. 7: a, E#23 (OD) measured with linear crossed polarization (crosses) and circular parallel polarization (circles), with LRT; b, E#71 (OS) measured with circular polarization (circles) and fluorescence mode (tri-

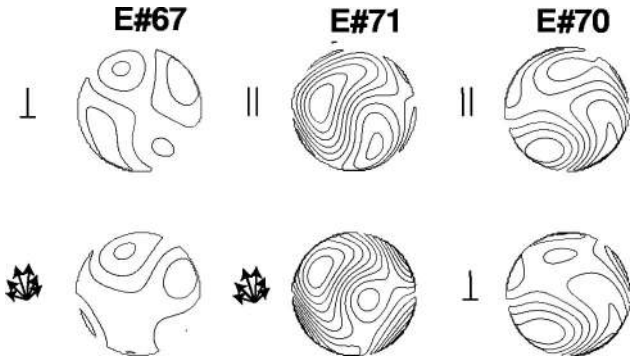

Fig. 7. Wave aberration contour maps for eyes #67, #71, and #70, measured with the S–H for polarization combinations as explained in Fig. 5. Lines are plotted every 0.2 μm. Defocus has been canceled. Pupil diameter was 6.5 mm for #67 and #71 and 6 mm for #70.

angles), with the S–H; c, E#67 (OS) measured with crossed linear polarization (crosses) and fluorescence mode (triangles), with the S–H; and d, E#70 (OS) measured with crossed linear polarization (crosses) and circular polarization (circles), with the S–H. Error bars indicate the mean standard deviation. The coefficient ordering and normalization follows the Optical Society of America standardization committee recommendations.[42] The Zernike coefficient patterns vary substantially across individuals, but measurements on the same subject differing only by the polarization states are very similar. Figure 9 shows examples of individual coefficients Z_2^0 (a), Z_2^{-2} (b), Z_3^1 (c), and Z_4^0 (d), for the 60 eyes and 2 experimental conditions of the LRT measurements (left panels) and the 11 eyes and 3 experimental conditions of the S–H measurements (right panels). Eyes are ranked by decreasing defocus coefficient (from higher to lower myopes).

Despite discrete and limited sampling of the wave aberration,[43] the Zernike polynomials can be considered practically orthogonal. We therefore performed a univariate statistical analysis (Student t-test) on each Zernike coefficient to assess possible differences across conditions rather than performing a multivariate analysis (Hotelling t-squared test) on Zernike sets.[44] This allows us to assess whether some particular coefficients are more likely to show differences. For the 60 eyes measured with the LRT, only 44 coefficients out of 1980 (60×33 terms), i.e., 2.2%, showed statistically significant differences (t-test, $p < 0.001$) between the linear crossed and circular parallel polarization. The defocus term (Z_2^0) was significantly different in seven eyes. This term along with Z_3^{-3} was the one showing differences in more eyes (8.5%). A least-square-difference multiple comparison test showed only significant differences ($p = 0.0002$) on the defocus term. The mean standard deviation of the Zernike coefficients (averaged across subjects and Zernike terms) was 0.065 μm, with averaging of the standard deviations obtained for each polarization state. When data from all polarization states was pooled, the mean standard deviation of the Zernike coefficients was 0.077 μm, only slightly higher than within the same polarization state. For the 11 eyes measured with the S–H, 37% of the coefficients showed statistically significant differences (t-test, $p < 0.001$) between linear crossed polarization

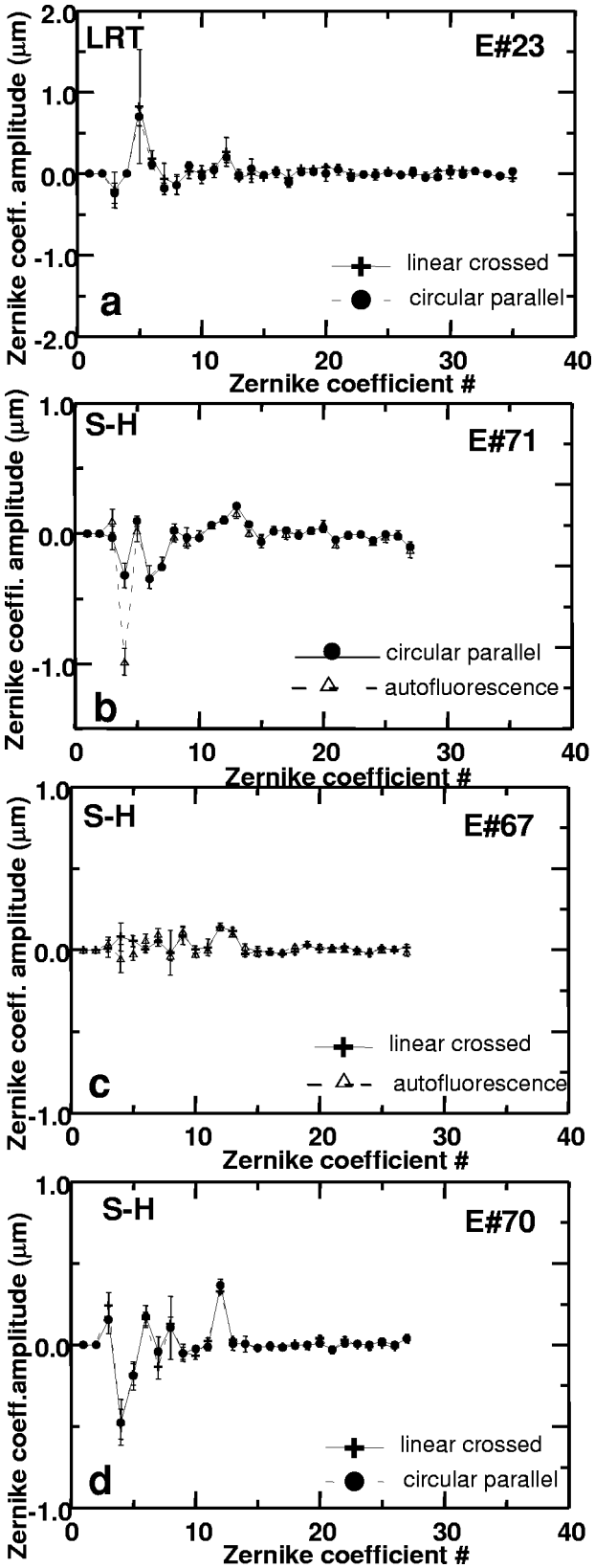

Fig. 8. Zernike coefficients for eye #23 from Fig. 6(a) and the three eyes (#71, #67, #70) from Fig. 7(b)–7(d), comparing different combinations of polarization conditions. Zernike order and normalization, following the OSA Standard Committee recommendations.[42] Each symbol is the average of several measurements in the same conditions. Error bars stand for the mean standard deviation.

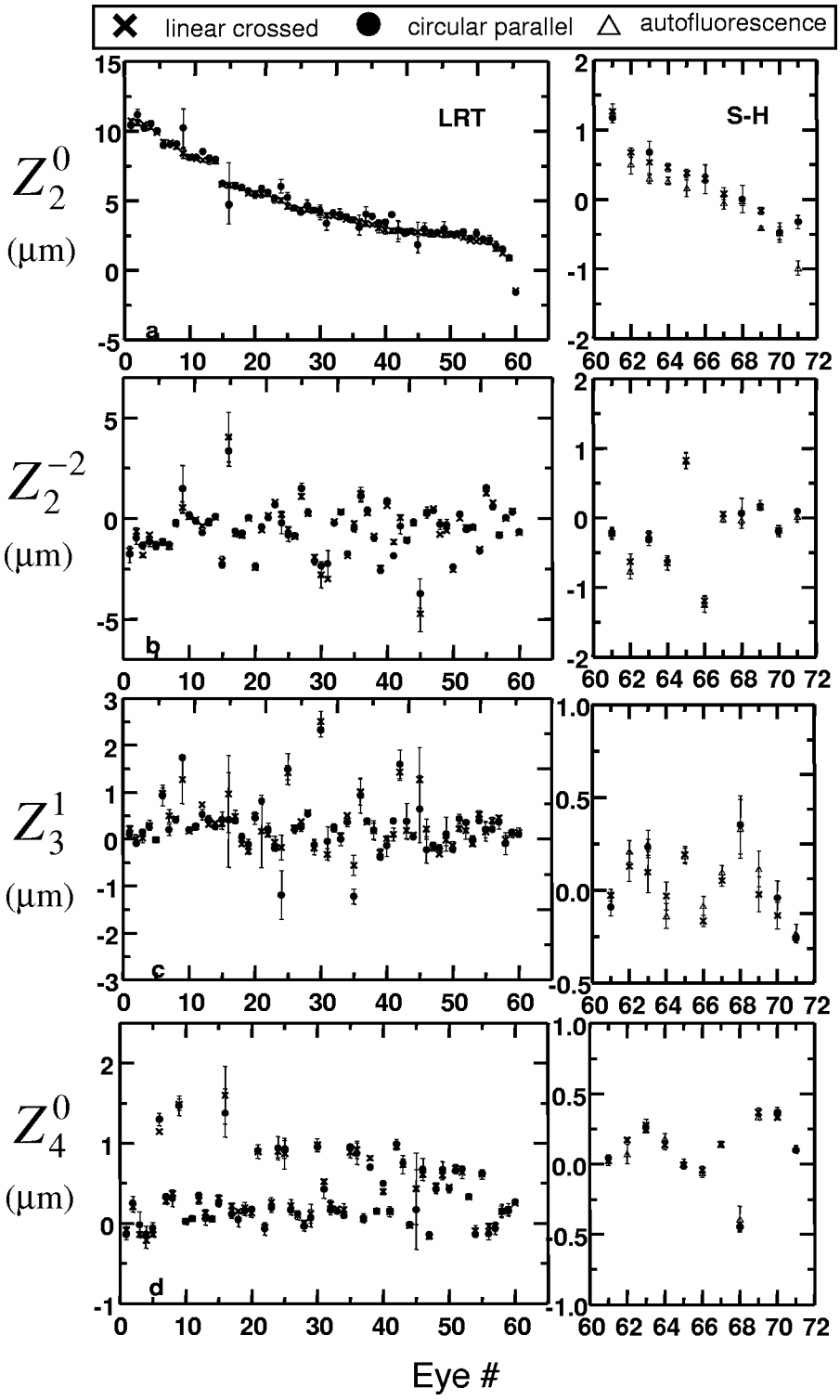

Fig. 9. Zernike coefficients: a, Z_2^0 (defocus); b, Z_2^{-2} (astigmatism at 90 deg); c, Z_3^1 (horizontal coma); d, Z_4^0 (fourth-order spherical aberration) for all eyes of this study (E#1–60 measured with LRT and E#61–71 with the S–H), comparing at least two different polarization states (represented by different symbols). Error bars stand for the mean standard deviation.

and autofluorescence, 37% between circular parallel and linear crossed polarization, and 46% between circular parallel polarization and autofluorescence. These differences are very likely due to differences in alignment between measurements and not differences intrinsic to the polarization state. Comparing sets of measurements under similar polarization conditions, but repositioning the subject between sets of ten consecutive runs, provided similar percentages of significantly different (t-test, $p < 0.001$) coefficients: 40% comparing linear crossed polarization sets of measurements, 52% for circular parallel polarization, and 60% for autofluorescence. The larger

variability of the autofluorescence data is likely due to the lower signal-to-noise ratio associated with this type of measurements.[31] The mean standard deviation of the Zernike coefficients (across all polarization conditions) was 0.126 μm, within a single polarization state it was 0.102 μm on average, and across identical consecutive runs it was 0.039 μm.

4. DISCUSSION

We have shown that when different states of polarization are used in the illumination and the detection channels, the intensity of the retinal images captured by imaging aberrometers depends on the position over the pupil of the entry (or exit) ray. However, we found that within the accuracy and limited sampling density of the technology used, this polarization has little effect on the aberrations measured. The fact that ocular aberrations measured with imaging methods, such as LRT or the S–H, are insensitive to polarization has important practical implications. For example, when building such an instrument, one can choose the polarization states for illumination and detection that result in the best light-efficient configuration, or that avoids reflections or artifacts. This differs from the case of conventional double-pass measurements, where differences in polarization produced variations in the point-spread and modulation transfer functions.[26,45,46] Recent data obtained with the spatially resolved refractometer also show that ocular aberrations do not depend on the state of polarization.[25] This is a psychophysical technique, and the subjects did not perceive differences as a linear polarizer in the test channel was moved, for any of the pupil locations under test. These results, along with those shown in the present study, suggest that the differences in retardation across the pupil imposed by corneal birefringence, produce nonsignificant phase delays compared with those produced by aberrations, at least within the accuracy of the measurements. Interestingly, these results also hold for patients following LASIK surgery. Along with a change in corneal shape, producing a significant increase of aberrations,[29] these patients may have suffered a change in corneal birrefringence as a result of reorganization of stromal collagen fibrils induced by surgery.[47–49] Even if only a fraction of stromal fibers undergo reorganization, the stromal bed is substantially reduced in the higher-myopia patients. However, the intensity distribution patterns obtained by LRT do not change with surgery (for neither crossed linear nor parallel circular polarizations). More sophisticated ellipsometric techniques and improved wave-front sensing techniques may allow us in the future to capture more subtle polarization-related differences.

ACKNOWLEDGMENTS

The authors acknowledge contributions from Esther Moreno-Barriuso in the early stages of this study. Sergio Barbero helped with subject handling and data collection. Agustín Mayo (Universidad de Valladolid) gave advice on statistical analysis. This study was supported by grants TIC98-0925-C02-01 from the Ministerio de Educación y Cultura, Spain; CAM 08.7/0010./2000 from the Comunidad Autónoma de Madrid, Spain; CONACyT 110670 predoctoral fellowship from Consejo Nacional de Ciencia y Tecnología, Mexico, to conduct work at Imperial College, London; EPSRC GR/M27043 from the Engineering and Physical Sciences Research Council, UK; and a British Council travel grant.

Corresponding author Susana Marcos can be reached by e-mail at susana@io.cfmac.csic.es

REFERENCES

1. J. Liang, D. R. Williams, and D. T. Miller, "Supernormal vision and high-resolution retinal imaging through adaptive optics," J. Opt. Soc. Am. A **14**, 2884–2892 (1997).
2. L. Zhu, P. Sun, D. Bartsch, W. R. Freeman, and Y. Fainman, "Adaptive control of a micromachined continuous-membrane deformable mirror for aberration compensation," Appl. Opt. **38**, 168–176 (1999).
3. R. Navarro, E. Moreno-Barriuso, S. Bará, and T. Mancebo, "Phase-plates for wave-aberration compensation in the human eye," Opt. Lett. **25**, 236–238 (2000).
4. S. M. MacRae, J. Schwiegerling, and R. Snyder, "Customized corneal ablation and super vision," J. Refract. Surg. **16**, 230–235 (2000).
5. H. Hofer, L. Chen, G. Yoon, B. Singer, Y. Yamauchi, and D. Williams, "Improvement in retinal image quality with dynamic correction of the eye's aberrations," Opt. Express **8**, 631–643 (2001). http://www.opticsexpress.org/oearchive/source/31887.htm.
6. E. J. Fernandez, I. Iglesias, and P. Artal, "Closed-loop adaptive optics in the human eye," Opt. Lett. **26**, 746–748 (2001).
7. J. C. He, S. Marcos, R. H. Webb, and S. A. Burns, "Measurement of the wave-front aberration of the eye by a fast psychophysical procedure," J. Opt. Soc. Am. A **15**, 2449–2456 (1998).
8. J. Liang, B. Grimm, S. Goelz, and J. F. Bille, "Objective measurement of wave aberrations of the human eye with the use of a Hartmann–Shack wave-front sensor," J. Opt. Soc. Am. A **11**, 1949–1957 (1994).
9. J. Liang and D. R. Williams, "Aberrations and retinal image quality of the normal human eye," J. Opt. Soc. Am. A **14**, 2873–2883 (1997).
10. G. Walsh, W. N. Charman, and H. C. Howland, "Objective technique for the determination of monochromatic aberrations of the human eye," J. Opt. Soc. Am. A **1**, 987–992 (1984).
11. R. Navarro and M. A. Losada, "Aberrations and relative efficiency of light pencils in the living human eye," Optom. Vision Sci. **74**, 540–547 (1997).
12. P. Mierdel, H. E. Krinke, W. Wiegand, M. Kaemmerer, and T. Seiler, "Measuring device for determining monochromatic aberration of the human eye," Ophthalmologe **94**, 441–445 (1997).
13. E. Moreno-Barriuso, S. Marcos, R. Navarro, and S. A. Burns, "Comparing laser ray tracing, spatially resolved refractometer and Hartmann–Shack sensor to measure the ocular wavefront aberration," Optom. Vision Sci. **78**, 152–156 (2001).
14. T. Salmon, L. Thibos, and A. Bradley, "Comparison of the eye's wave-front aberration measured psychophysically and with the Shack–Hartmann wave-front sensor," J. Opt. Soc. Am. A **15**, 2457–2465 (1998).
15. F. C. Delori and K. P. Pfibsen, "Spectral reflectance of the human ocular fundus," Appl. Opt. **28**, 1061–1077 (1989).
16. N. Lopez-Gil and H. Howland, "Measurement of the eye's near infrared wave-front aberration using the objective crossed-cylinder aberroscope technique," Vision Res. **39**, 2031–2037 (1999).
17. L. Llorente, S. Marcos, S. Barbero, R. Navarro, and E. Moreno-Barriuso, "Ocular aberrations in infrared and vis-

ible light using a laser ray tracing technique," Invest. Ophthalmol. Visual Sci. Suppl. **41**, S87 (2001).
18. W. N. Charman and J. A. M. Jennings, "Objective measurements of the longitudinal chromatic aberration of the human eye," Vision Res. **16**, 999–1005 (1976).
19. S. Marcos, S. A. Burns, E. Moreno-Barriuso, and R. Navarro, "A new approach to the study of ocular chromatic aberrations," Vision Res. **39**, 4309–4323 (1999).
20. L. N. Thibos, M. Ye, X. X. Zhang, and A. B. Bradley, "The chromatic eye: a new reduced-eye model of ocular chromatic aberration in humans," Appl. Opt. **31**, 3594–3600 (1992).
21. G. J. Van Blokland and S. C. Verhelst, "Corneal polarization in the living human eye explained with a biaxial model," J. Opt. Soc. Am. A **4**, 82–90 (1987).
22. J. M. Bueno and M. C. W. Campbell, "Polarization properties for *in vivo* human lenses," Invest. Ophthalmol. Visual Sci. Suppl. **42**, S161 (2001).
23. G. J. V. Blokland and D. V. Norren, "Intensity and polarization of light scattered at small angles from the human fovea.," Vision Res. **26**, 485–494 (1986).
24. G. J. V. Blokland, "The optics of the human eye with respect to polarized light," Ph.D. thesis (University of Utrecht, Utrecht, The Netherlands, 1986).
25. P. M. Prieto, F. Vargas-Martin, J. S. McLellan, and S. A. Burns, "The effect of the polarization on ocular wave aberration measurements," J. Opt. Soc. Am. A **19**, 809–814 (2002).
26. J. M. Bueno and P. Artal, "Double-pass imaging polarimetry in the human eye," Opt. Lett. **24**, 64–66 (1999).
27. P. Artal, S. Marcos, R. Navarro, and D. R. Williams, "Odd aberrations and double-pass measurements of retinal image quality," J. Opt. Soc. Am. A **12**, 195–201 (1995).
28. R. Navarro and E. Moreno-Barriuso, "Laser ray-tracing method for optical testing," Opt. Lett. **24**, 1–3 (1999).
29. E. Moreno-Barriuso, J. Merayo-Lloves, S. Marcos, R. Navarro, L. Llorente, and S. Barbero, "Ocular aberrations before and after myopic corneal refractive surgery: LASIK-induced changes measured with laser ray tracing," Invest. Ophthalmol. Visual Sci. **42**, 1396–1403 (2001).
30. E. Moreno-Barriuso and R. Navarro, "Laser ray tracing versus Hartmann–Shack sensor for measuring optical aberrations in the human eye," J. Opt. Soc. Am. A **17**, 974–985 (2000).
31. H. L. Diaz Santana and J. C. Dainty, "Single-pass measurements of the wave-front aberrations of the human eye by use of retinal lipofuscin autofluorescence," Opt. Lett. **24**, 61–63 (1999).
32. L. Diaz-Santana Haro, "Wavefront sensing in the human eye with a Shack–Hartmann sensor," Ph.D. thesis (Imperial College of Science Technology and Medicine, London, 2000).
33. F. Delori, C. K. Dorey, G. Staurenghi, O. Arend, D. G. Goger, and J. J. Weiter, "*In vivo* fluorescence of the ocular fundus exhibits retinal pigment epithelium lipofuscin characteristics," Invest. Ophthalmol. Visual Sci. **36**, 718–729 (1995).
34. J. Bueno and P. Artal, "Polarization and retinal image quality estimates in the human eye," J. Opt. Soc. Am. A **18**, 489–496 (2001).
35. S. A. Burns, S. Wu, F. Delori, and A. E. Elsner, "Direct measurement of human-cone-photoreceptor alignment," J. Opt. Soc. Am. A **12**, 2329–2338 (1995).
36. A. Stanworth and E. J. Naylor, "The polarization optics of the isolated cornea," Br. J. Ophthamol. **34**, 201–211 (1950).
37. W. T. Cope, M. L. Wolbarsht, and B. S. Yamanashi, "The corneal polarization cross," J. Opt. Soc. Am. **68**, 1139–1141 (1978).
38. B. F. Hocheimer and H. A. Kues, "Retinal polarization effects," Appl. Opt. **21**, 3811–3818 (1982).
39. S. Marcos and S. A. Burns, "Cone spacing and waveguide properties from cone directionality measurements," J. Opt. Soc. Am. A **16**, 995–1004 (1999).
40. S. Marcos, E. Moreno-Barriuso, R. Navarro, and L. Llorente, "Retinal reflectivity in laser ray tracing measurements: What can we learn apart from ocular aberrations?" Presented at the OSA 2000 Annual Meeting, October 22–26, Providence, R.I., 2000.
41. S. A. Burns, J. C. He, and F. C. Delori, "Do the cones see light scattered from the deep retinal layers," *Vision Science and Its Applications*, Vol. 1 of 1997 OSA Technical Digest Series (Optical Society of America, Washington, D.C., 1997), pp. 94–97.
42. L. N. Thibos, R. A. Applegate, J. T. Schwiegerling, R. H. Webb, and V. S. T. Members, "Standards for reporting the optical aberrations of eyes," in *Vision Science and Its Applications*, Vol. 35 of OSA Trends in Optics and Photonics Series (Optical Society of America, Washington, D.C., 2000), pp. 110–130.
43. J. Y. Wang and D. E. Silva, "Wave-front interpretation with Zernike polynomials," Appl. Opt. **19**, 1510–1518 (1980).
44. R. R. Sokal and F. J. Rohlf, *Biometry: The Principles and Practice of Statistics in Biological Research*, 3rd ed. (Freeman, New York, 1995).
45. J. M. Gorrand, R. Alfieri, and J. Y. Boire, "Diffusion of the retinal layers of the living human eye," Vision Res. **24**, 1097–1106 (1984).
46. J. Gorrand, "Diffusion of the human retina and quality of the optics of the eye on the fovea and the peripheral retina," Vision Res. **19**, 907–912 (1979).
47. R. A. Farrell, J. F. Wharam, D. Kim, and R. L. McCally, "Polarized light propagation in corneal lamellae," J. Refract. Surg. **15**, 700–705 (1999).
48. K. M. Meek and R. H. Newton, "Organization of collagen fibrils in the corneal stroma in relation to mechanical properties and surgical practice," Refract. Surg. **15**, 695–699 (1999).
49. R. Brinkmann, B. Radt, C. Flamm, J. Kampmeier, N. Koop, and R. Birngruber, "Influence of temperature and time on thermally induced forces in corneal collagen and the effect on laser thermokeratoplasty," J. Cataract Refract. Surg. **26**, 744–754 (2000).